Quaternary Research 81 (2014) 433–444

Contents lists available at ScienceDirect

Quaternary Research

journal homepage: www.elsevier.com/locate/yqres

Magnetic parameter variations in the Chaona loess/paleosol sequences in the central Chinese Loess Plateau, and their significance for the middle Pleistocene climate transition

Yougui Song [a,b,*], Xiaomin Fang [b,c], John W. King [d], Jijun Li [b], Ishikawa Naoto [e], Zhisheng An [a]

[a] State Key Laboratory of Loess and Quaternary Geology, Institute of Earth and Environment, Chinese Academy of Sciences, Xi'an 710075, China
[b] Key Laboratory of Western China's Environmental Systems, Ministry of Education of China, Lanzhou 730000, China
[c] Key Laboratory of Continental Collision and Plateau Uplift, Institute of Tibetan Plateau Research, Chinese Academy of Sciences, Beijing 100085, China
[d] Graduate School of Oceanography, University of Rhode Island, Narragansett, RI 02882, USA
[e] Graduate School of Human and Environmental Studies, Kyoto University, Kyoto 606-8501, Japan

ARTICLE INFO

Available online 29 October 2013

Keywords:
Rock magnetism
Loess–paleosol sequence
East Asian monsoon history
Middle-Pleistocene climatic transition

ABSTRACT

A high-resolution rock magnetic investigation was performed on the Chaona Quaternary loess/paleosol sequences in the Central Chinese Loess Plateau. Based on a newly developed independent unturned time scale and magnetic records, we reconstructed the history of the East Asia monsoons during the last 3 Ma and explored the middle Pleistocene climate transition (MPT). Rock magnetic results show that the loess layers are characterized by relatively high coercivity and remanent coercivity, lower magnetic susceptibility (MS), and that the paleosol layers are characterized by relatively high MS, saturation magnetization and remanent saturation magnetization. Spectrum analyses indicate that there are various periods in addition to orbital periodicities. According to the onset and stable appearance of 100 kyr period, we consider that the MPT recorded in this section began at ~1.26 Ma and was completed by ~0.53 Ma, which differs from previous investigations based on orbitally tuned time scales. The forcing mechanism for the MPT was more complicated than just the orbital forcing. We conclude that the rapid uplift of the Tibetan Plateau may have played an important role in the shift of periodicities during the middle Pleistocene.

Introduction

The Chinese Loess Plateau (CLP) is of major interest to Quaternary geologists because its loess–paleosol sequences have been commonly regarded as the most complete and reliable terrestrial archive of paleoclimatic and environmental change (Heller and Liu, 1986; Liu et al., 1986; Kukla, 1987; An et al., 1990; An, 2000; Hao et al., 2012). In typical Chinese loess sequences, paleosols always have higher magnetic susceptibility (MS) than loesses. MS is regarded as a proxy for the intensity of the summer monsoon (An et al., 1991; An, 2000) and paleo-precipitation (Heller et al., 1993; Maher et al., 1994; Maher and Thompson, 1995; Evans et al., 2002). Continuous, high-resolution magnetic measurements, such as MS, frequency-dependence of susceptibility (χ_{fd}), isothermal remanent magnetization (IRM), and anhysteretic remanent magnetization (ARM), have been widely reported and interpreted in terms of paleoclimatic and tectonic events (Kukla, 1987; Maher and Thompson, 1992; An et al., 2001; Liu et al., 2007; Nie et al., 2008a; Hao et al., 2012). However, currently there are no high-resolution hysteresis parameter records that can provide important new insights into climate change in terms of the magnetic mineralogy.

The middle Pleistocene climate transition (MPT), which was marked by a shift from the previously dominant 41-kyr cycles to the more recently dominant 100-kyr cycles roughly in the middle Pleistocene, brought the global climate system into the late Pleistocene ice ages (Ruddiman et al., 1989; Mudelsee and Schulz, 1997; Berger et al., 1999; Schmieder et al., 2000; Clark et al., 2006). The process and origin of the MPT remain of persistent interest and conjecture and have been extensively documented within the oceanic realm (Clark et al., 2006). However, there are very few reports on the MPT in the CLP (Heslop et al., 2002; Han et al., 2012), although a substantial amount of literature related to loess paleoclimatic changes has been published. Fang et al. (1999) suggest that the initiation of the MPT occurred at ~0.8 Ma in the loess and was driven by the uplift of the Tibetan plateau. Unfortunately, the basal age of the section they studied is just 0.8 Ma and thus did not span the entire MPT. Heslop et al. (2002) first explored the timing and structure of the MPT in the Luochuan loess section. Comparing the MS and grain-size time series with the ODP 677 $\delta^{18}O$ curve, they concluded that the MPT interval occurred between 920 ka (MIS22/23) and 620 ka (MIS15/16). Recently, Han et al. (2012) used high-resolution astronomically tuned MS and grain-size records from the Chaona loess–paleosol sequence to reveal a remarkable two-step

* Corresponding author at: State Key Laboratory of Loess and Quaternary Geology, Institute of Earth and Environment, Chinese Academy of Sciences, Xi'an 710075, China.
E-mail addresses: ygsong@loess.llqg.ac.cn, syg@ieecas.cn (Y. Song).

0033-5894/$ – see front matter © 2013 University of Washington. Published by Elsevier Inc. All rights reserved.
http://dx.doi.org/10.1016/j.yqres.2013.10.002

simultaneous enhancement of the East Asian summer and winter monsoons at 0.9 Ma and 0.64 Ma, respectively, which was attributed to the MPT. However, their analysis was based on an orbitally tuned time scale, as the $\delta^{18}O$ of ODP 677 is regarded as one of the target curves for orbital tuning. It is a questionable, possibly circular, practice to use an orbitally tuned time series to examine orbital periodicities (Lu et al., 2004). Lu et al. (2004) improved an independent grain-size climate-proxy-based age model originally developed by Porter and An (1995). In this paper, we present a high-resolution rock magnetic record from the Quaternary loess–paleosol sequence of the central CLP and analyze the spectral behavior of various rock magnetic parameters dated using the new age model. We then discuss the timing and structure of the MPT.

Setting and stratigraphy

The studied loess–paleosol section is located near the town of Chaona (107°12′ E. 35°7′ N), Gansu Province, on the central CLP (Fig. 1). The present climate is dominated by the East Asia monsoon, with warm and humid summers and cold and dry winters. The well-exposed loess–paleosol sequence is approximately 175 m thick and contains a complete Quaternary eolian sequence of 33 pairs of loesses and paleosols (Fig. 2). The stratigraphic markers S5, L9 and L15 in the CLP are well exposed in a cliff outcrop. Paleosol S5 is located at a depth of 32.5–37.5 m and is composed of three sub-paleosol horizons interbedded with two loess sub-layers. Marker L9, located at a depth of 54–64.6 m, is light brown, massive, and much coarser than other younger loess layers; whereas L15, located at a depth of 82.9–88.5 m, is yellowish, loose, massive, and very coarse silt and contains large numbers of carbonate nodules. The basal paleomagnetic age of this loess–paleosol sequence is 2.6 Ma (Song et al., 2001). Underlying the loess–paleosol is a red clay sequence that is 125 m thick and accumulated between 8.1 Ma and 2.6 Ma (Song et al., 2007)

Methods

Magnetic measurements

The dried individual samples, which were collected at 10-cm intervals, were analyzed for MS. These analyses were performed using a Bartington MS2 susceptometer at frequencies of 470 Hz (i.e., χ_{lf}) and 4700 Hz (i.e. χ_{hf}) at Lanzhou University. $\Delta\chi$ ($\Delta\chi = \chi_{lf} - \chi_{hf}$) and χ_{fd} [$\chi_{fd} = (\chi_{lf} - \chi_{hf})/\chi_{lf}{}^{*}100$] represent the absolute and relative behavior, respectively, of the frequency-dependent susceptibility. A total of 659 samples obtained at 20–40 cm intervals with an average time resolution of 4.5 ka were selected for hysteresis analysis. Powder samples weighing 10–30 mg were wrapped in thin aluminum foil and measured for magnetic hysteresis parameters, including saturation magnetization (M_s), remanent saturation magnetization (M_r), and coercivity (B_c). We measured the hysteresis parameters using a Princeton Measurements MicroMag 2900-02C alternating gradient force magnetometer with a maximum field of 1 T at the Paleomagnetism and Rock Magnetism Laboratory of Kyoto University. The M_s, M_r and B_c were determined on the slope-corrected hysteresis loops. The remanent coercivity (B_{cr})

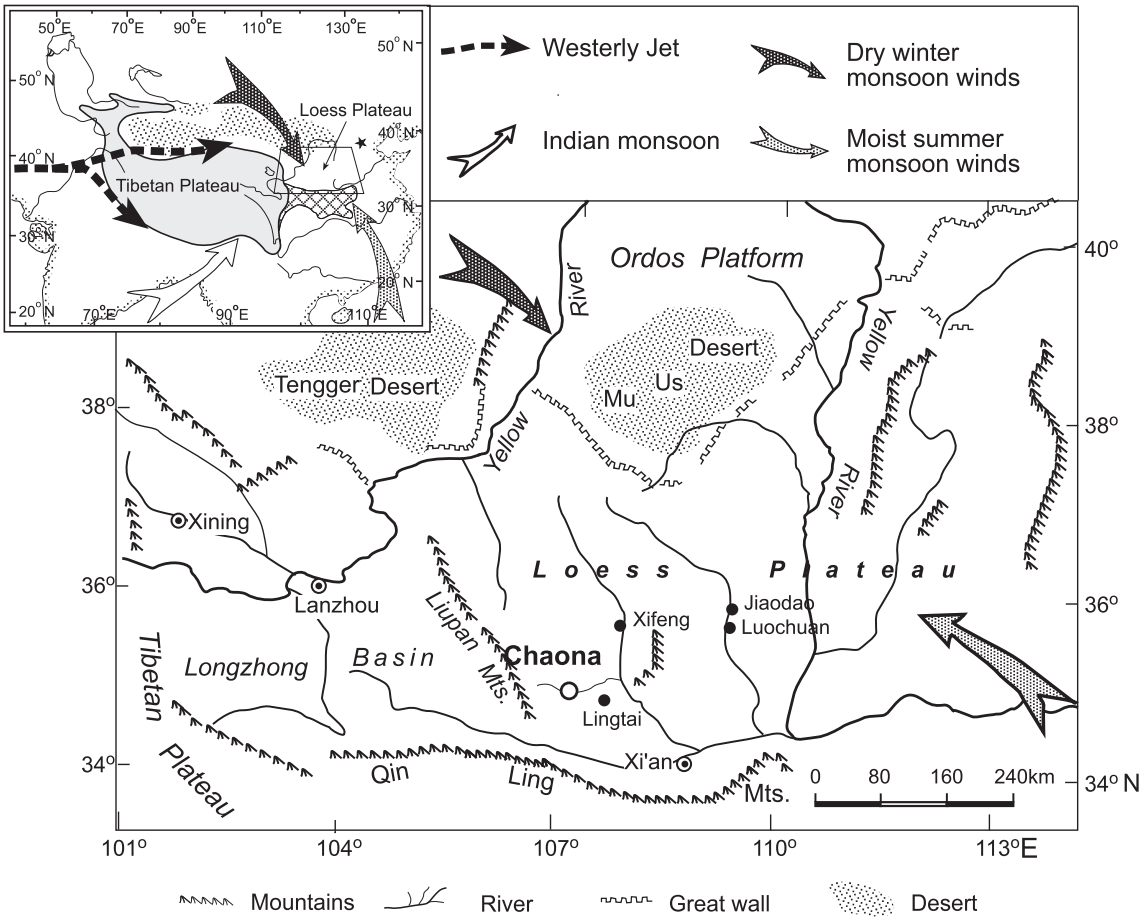

Figure 1. Schematic map showing the physical geography of the Chinese Loess Plateau and locations of the Chaona section (modified from Song et al., 2007). The inset illustrates the location of the Chinese Loess Plateau in relation to Tibet and the modern Asian air-circulation pattern.

https://doi.org/10.1016/j.yqres.2013.10.002 Published online by Cambridge University Press

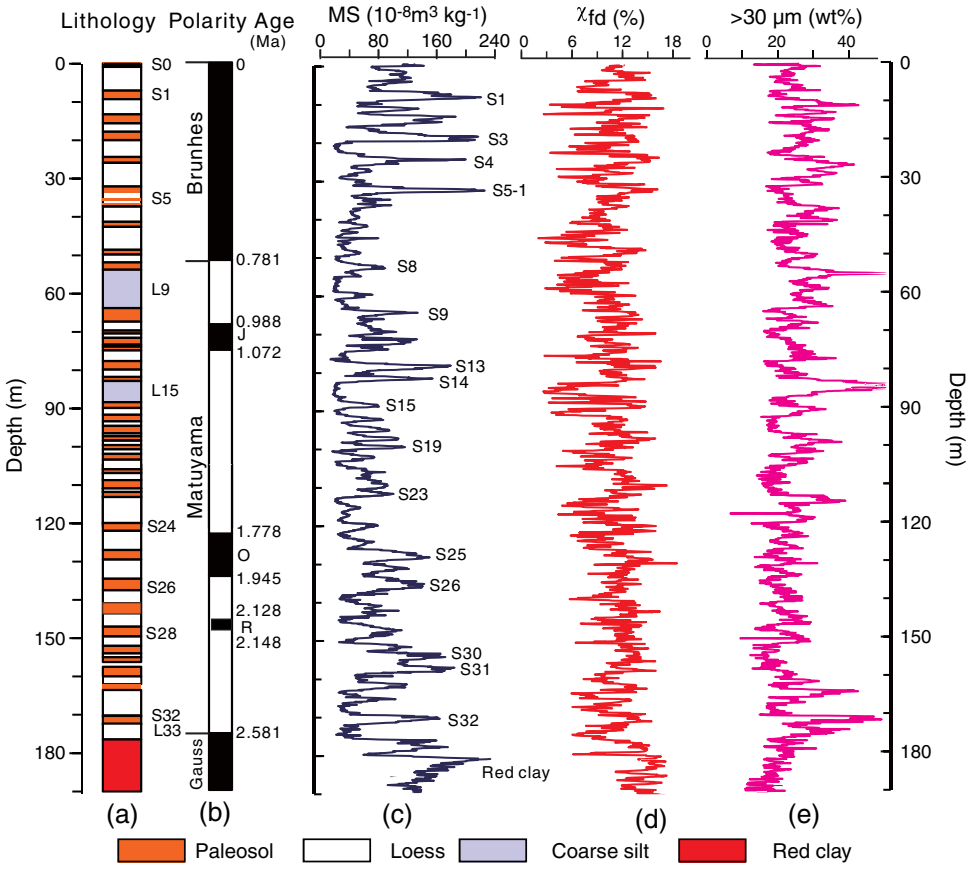

Figure 2. Lithology, polarity, magnetic susceptibility (MS), frequency-dependence susceptibility (χfd) and grain-size (the concentration of >30 μm particles) variations in the Chaona section in the central Chinese Loess Plateau. Magnetostratigraphy is from Song et al (2001).

was measured by applying a maximum field of 1.0 T followed by a succession of increasing backfields. The saturation isothermal remanent magnetization was determined at 1 T (SIRM), −100 mT ($IRM_{-100\ mT}$) and −300 mT ($IRM_{-300\ mT}$). The $S_{-0.3\ T}$ is defined as $-IRM_{-300\ mT}$/SIRM. The isothermal remanent magnetization (HIRM) parameter was defined as $(SIRM + IRM_{-300\ mT})/2$ (Thompson and Oldfield, 1986).

Age-model development

Various studies have used the indications of Earth's orbital periodicities in the Chinese loess deposits to develop age models based on tuning to such targets as orbital composites or the marine oxygen isotope record (Ding et al., 1994; Lu et al., 1999, 2003; Heslop et al., 2000; Sun et al., 2006b; Han et al., 2011). This approach may be good for establishing a time scale for studies of environmental change. However, it is circular and questionable to use a record with a tuned time scale to examine temporal variations in orbital forcing (Lu et al., 2004).

Here, we present a relatively independent time scale based on a grain-size age model (Porter and An, 1995; Lu et al., 2004). Lu et al. (2004) discussed the assumptions behind the use of this approach. First, many absolute dating efforts across the CLP have demonstrated that the first loess unit (L1), and the first reddish paleosol unit (S1) in the upper part of the loess section were formed during the last glacial (72 ~ 12 ka) and interglacial periods (126–72 ka), respectively (Lu et al., 2007). According to the new standard time scale (ANTNS2004) (Lourens et al., 2004), the paleomagnetic ages of the Brunhes/Matuyama (B/M) at 51.5 m and the Matuyama/Gauss (M/Ga) at 175 m (Song et al., 2001) are 0.781 and 2.581 Ma, respectively, and the Jaramillo and Olduvai subchrons span the intervals of 0.988 to 1.072 Ma and 1.778 to 1.945 Ma, respectively (Fig. 2).

Second, the age of each sampling level is interpolated by using a grain-size age model (Porter and An, 1995).

$$T_m = T_1 + (T_2 - T_1)\left(\sum_{i=1}^{m} A_i^{-1} / \sum_{i=1}^{n} A_i^{-1}\right),$$

where T_1 and T_2 are the age control points. The age control points are based on 'absolute' dating and magnetostratigraphy. A_i is the accumulation rate at level *i*, which is assumed to be proportional to the content of the >30-μm particles; *n* is the total sampling level between T_1 and T_2; and m is the sampling level at T_1 and T_2.

Results

Magnetic measurements

The shapes of the hysteresis loops may be an indicator of the degree of pedogenesis. A selection of typical magnetic hysteresis loops and parameters is shown in Fig. 3 and Table 1, respectively. It is clear that the hysteresis properties of the loess and paleosols differ significantly. The average values of χ_{lf}, χ_{hf}, M_r and M_s in the paleosols are roughly double those in the loess, whereas the average values of B_{cr} and B_c are higher in the loess. The average value of χ_{fd} in the paleosols, however, is very near that in the loess (Table 1). The loess samples with low susceptibility show slightly constricted loops with larger widths (Fig. 3a, Table 1). The loops do not close at 0.5 T, which suggests

https://doi.org/10.1016/j.yqres.2013.10.002 Published online by Cambridge University Press

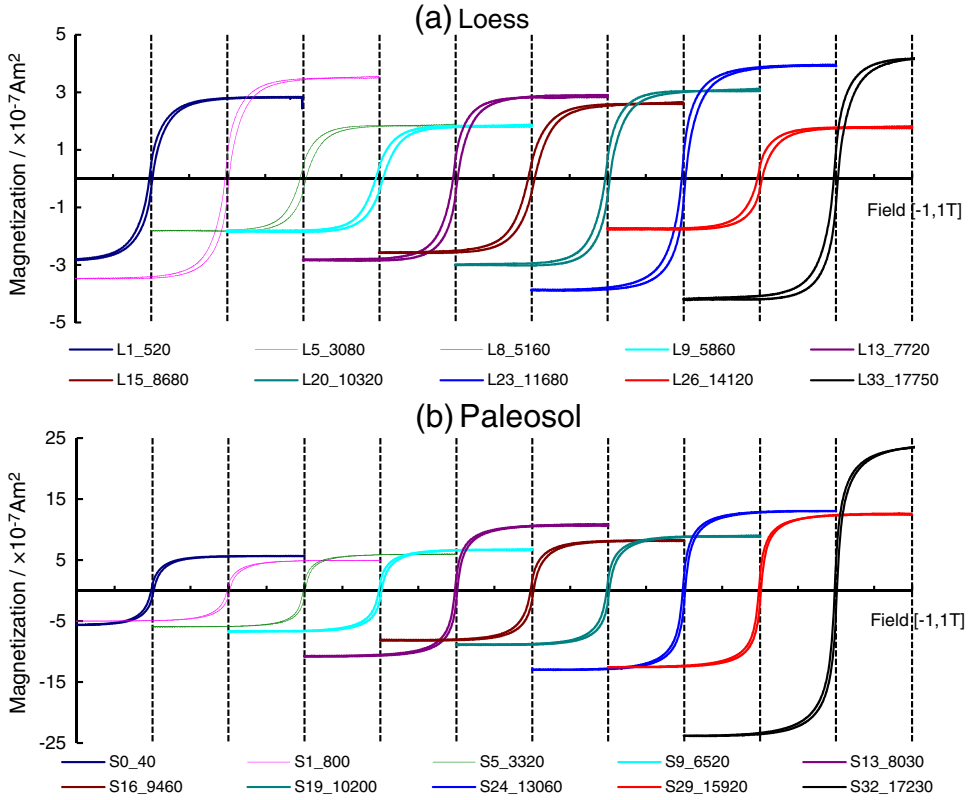

Figure 3. Typical magnetic hysteresis loops of loess and paleosols samples from the Chaona section.

significant amounts of antiferromagnetic minerals, e.g., hematite or goethite. Constriction appears for the loess samples with intermediate or larger values of MS (Fig. 3a). These hysteresis loops are narrower, particularly in the middle of the loops, resulting in constricted shapes. The paleosol samples with high MS display narrow hysteresis loops, and the constriction is largely suppressed. Most of the paleosol loops close at 0.3 T (Fig. 3b), indicating higher concentrations of ferrimagnetic minerals (e.g., magnetite and maghemite).

Previous rock-magnetism studies indicate that the values of M_r and M_s are closely related to the type and content of magnetic minerals (King and Channell, 1990; Hunt et al., 1995; Dunlop and Özdemir, 1997; Fukuma and Torii, 1998; Bloemendal and Liu, 2005; Deng et al., 2005a). Higher M_r (M_s) values indicate an increase in ferrimagnetic minerals, such as magnetite and maghemite, and lower values imply the absence of strongly ferrimagnetic minerals. The high coercivity (B_c, B_{cr}) may imply the presence of antiferromagnetic goethite and

Table 1
Magnetic hysteresis parameters of typical loess and paleosol samples (hysteresis loops are shown in Fig. 3).

Stratum	Sample no	χ_{lf}	χ_{hf}	χ_{fd}	B_{cr}	B_c	M_r	M_s	SIRM	HIRM	$S_{-0.3\,T}$
		$10^{-8}m^3kg^{-1}$	$10^{-8}m^3kg^{-1}$	%	mT	mT	$10^{-3}Am^2kg^{-1}$	$10^{-3}Am^2kg^{-1}$	$10^{-2}Am^2kg^{-1}$	$10^{-2}Am^2kg^{-1}$	
L1	480	124.34	113.54	8.68	27.91	8.82	12.37	78.60	1.18	0.04	0.93
L1	520	92.12	86.42	6.19	32.12	10.09	10.14	59.58	0.98	0.02	0.95
L5	3080	55.26	50.65	8.33	44.70	13.05	6.57	32.49	0.64	0.04	0.86
L8	5160	27.71	24.88	10.20	62.14	19.63	4.24	17.91	0.41	0.03	0.84
L9	5840	21.60	20.97	2.94	64.70	24.01	2.58	8.93	0.26	0.01	0.90
L13	7720	34.36	30.54	11.11	50.89	15.00	5.32	23.85	0.52	0.04	0.85
L15	8680	18.73	18.22	2.70	64.26	21.35	4.49	22.41	0.44	0.04	0.83
L20	10320	27.73	24.20	12.73	52.73	15.07	3.80	17.65	0.37	0.04	0.81
L23	11680	38.91	36.89	5.19	44.12	12.70	5.67	27.26	0.56	0.05	0.83
L26	14120	26.69	25.86	3.13	52.88	15.19	3.74	16.68	0.36	0.03	0.83
L33	17750	34.07	30.93	9.23	45.17	13.27	4.61	20.77	0.44	0.04	0.82
Loess (n = 368)		**50.52**	**45.27**	**9.84**	**43.23**	**13.01**	**5.57**	**28.50**	**0.54**	**0.04**	**0.87**
S0	40	126.49	113.91	9.95	26.01	8.10	11.35	67.51	1.08	0.04	0.92
S1	800	170.43	141.13	17.19	25.12	8.37	14.73	85.57	1.40	0.04	0.94
S5	3320	231.59	184.43	20.36	21.26	7.26	11.96	66.61	1.11	0.04	0.93
S9	6520	114.84	100.81	12.22	26.14	8.76	11.15	59.79	1.09	0.05	0.90
S13	8030	155.53	123.49	20.60	23.11	7.48	14.63	82.40	1.41	0.08	0.89
S16	9460	82.92	72.37	12.73	31.56	9.74	8.56	45.47	0.39	0.02	0.88
S19	10200	100.62	88.28	12.27	26.30	8.54	10.14	54.41	0.98	0.06	0.87
S24	13060	133.03	112.87	15.15	22.95	7.40	12.03	68.78	1.16	0.07	0.87
S29	15920	172.02	149.11	13.32	20.94	7.00	15.06	84.80	1.46	0.09	0.88
S32	17230	161.03	140.78	12.57	22.09	7.07	13.42	77.68	1.30	0.08	0.87
Paleosol (n = 245)		**107.06**	**93.45**	**12.46**	**28.15**	**8.84**	**9.36**	**51.18**	**0.91**	**0.05**	**0.88**

https://doi.org/10.1016/j.yqres.2013.10.002 Published online by Cambridge University Press

hematite (Fukuma and Torii, 1998). The B_c values of typical loess samples may exceed 20 mT, which is approximately 2–3 times higher than those of the paleosol samples (Table 1), which is higher than the B_c values of pure single-domain magnetite (10 mT) and lower than those of pure hematite (400 mT). The B_c of marker S5 is less than 10 mT, suggesting that either there are multi-domain grains or a high proportion of super-paramagnetic ferrimagnetic grains. The M_s and M_r values in the paleosol samples are typically significantly higher than those in the loess (Table 1). The value of M_r/M_s was plotted against B_{cr}/B_c on a so-called 'Day plot' (Day et al., 1977). All points fall in the pseudo-single domain region and are well-clustered but slightly spread along the B_{cr}/B_c axis (Fig. 4). The rock magnetic behavior indicates that the magnetic minerals in the loess layers are dominated by high-coercivity antiferromagnetic minerals with high values of B_c, B_{cr} and MS, and the paleosol layers have low-coercivity ferrimagnetic minerals, such as magnetite with high values of M_r, M_s and MS. These statistics confirm those of previous rock magnetic investigations (Liu et al., 1992, 2007; Hunt et al., 1995; Dekkers, 1997; Fang et al., 1999; Evans and Heller, 2001; Deng et al., 2005b).

Mineral magnetic time series

Detailed rock magnetic parameters, selected inter-parametric ratios, grain size (Lü et al., 2001), and stacked global $\delta^{18}O$ values (LR04) (Lisiecki and Raymo, 2005) are shown in Fig. 5. The following observations are noteworthy: (i) The paleosols (~interglacial stages) show higher ferrimagnetic (χ_{lf}, M_r, M_s, SIRM) and canted antiferromagnetic (HIRM) mineral concentrations and finer ferrimagnetic grain sizes (higher χ_{fd}) compared with the less weathered loess (~glacial) layers. The strongest paleosol development, in terms of maximum values of the magnetic parameters, occurred during the past 530 ka (S5-1). (ii) The general trend of the χ_{fd}, M_r, M_s and SIRM/HIRM curves is similar to that of MS, although the highest values of susceptibility appear in S5 rather than in S1. There is an approximately inverse relationship between B_{cr}, B_c, and MS, and the highest coercivity values were observed in markers L15 and L9. (iii) The $S_{-0.3\,T}$ curve shows an increasing trend since 2.6 Ma, which indicates a long-term increase in the proportion of ferrimagnetic relative to antiferromagnetic minerals. (iv) The long-term trend of HIRM and χ_{fd} is similar to that of LR04.

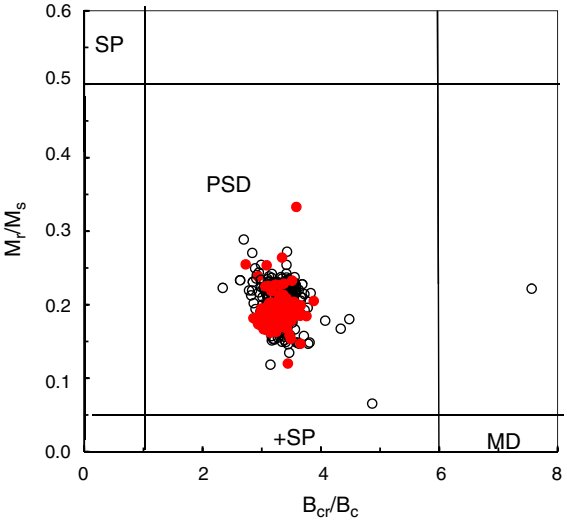

Figure 4. Day plot of the ratio of saturation remanence and saturation magnetization (M_r/M_s) and remanent coercivity and coercivity (B_{cr}/B_c) in the Chaona section. (Open circles denote loess samples, $n = 368$. Solid circles denote paleosol samples, $n = 245$).

Spectrum analysis

To identify possible intervals of spectrum change, we performed a wavelet analysis (Torrence and Compo, 1998) (Fig. 6). In general, the variation observed using the grain-size age model (Figs. 6a–d) differs from that based on the orbitally tuned time scale (Sun et al., 2006b) (Figs. 6e, f). For example, the ~100-kyr period of the stacked MS was very clear after ~0.6 Ma (Fig. 6e), but the ~100-kyr period in the Chaona MS appeared at approximately 0.53 Ma (Fig. 6a). Furthermore, there are no clear and significant orbital periods of χ_{fd} (Fig. 6b). The spectra of the MS and M_s (Figs. 6a, d) are similar and exhibit significant periods that are less than 128 kyr during the Quaternary Period. The orbital periods ~100 and 40 kyr occurred at ~1.2 Ma and then disappeared at ~1.0 Ma, but the ~100- kyr period occurred again at ~0.53 Ma.

Table 2 shows both orbital (~100 and 40-kyr) and non-orbital periods (~200 and 32-kyr) and related orbital periods of 400 and 70–80-kyr in the loess record, which differ from the standard orbital forcing spectrum. Fig. 7 shows that certain periods are not significant orbital periods above the 80% confidence level, particularly during the 0.5–1 Ma and 0–2.6 Ma time intervals. The ~100-kyr period occurred between 0.9 and 1.4 Ma, disappeared during the 0.5–1 Ma interval, except for B_c, and then reappeared at 0.6 Ma.

Discussion

Paleoclimatic interpretations of rock magnetic parameters

The eolian sediments in the CLP are closely related to the evolution of the East Asian monsoon system (An et al., 1990, 1991, 2001; Song et al., 2007; Maher et al., 2009); The MS and grain sizes of the loess–paleosol sequences have been regarded as sensitivity indexes to the intensities of the East Asian summer and winter monsoons, respectively (An et al., 1991, 2001; Porter and An, 1995; Fang et al., 1999; Han et al., 2012). We observed that the paleosol samples have higher MS, M_r, M_s, SIRM, HIRM and $S_{-0.3\,T}$, and the loess samples only have higher B_{cr} and B_c, which are similar to those of the Jiaodao loess–paleosol sequence (Deng et al., 2005b). In other words, the magnetic mineral assemblage in the loess layers is dominated by high-coercivity antiferromagnetic minerals, and the paleosol layers are dominated by low-coercivity ferrimagnetic minerals. Whereas the higher coercivity ('harder') component is thought to be of detrital origin, the lower coercivity ('softer') component was most likely formed in situ by (bio-) chemical processes (Zhou et al., 1990; Maher and Tompson, 1992; Bloemendal and Liu, 2005).

It is well documented by numerous studies that the antiferromagnetic minerals in the loess on the CLP are hematite and goethite, which are primarily transported from the Gobi desert by the East Asia winter monsoon (Hao et al., 2009; Nie et al., 2010). When the winter monsoon strengthens, the grain size of the eolian sediments becomes coarser (Fig. 5) and the total amount of eolian sediments increases, which in turn causes the increase in the proportion of antiferromagnetic minerals. Therefore, in a sense, the changes in B_{cr} and B_c are related to the winter monsoon intensity in the same manner as grain size. During interglacial periods, the East Asian summer monsoon prevailed over the CLP, dust concentrations decreased considerably, and warm and wet climate conditions facilitated pedogenesis. This led to high concentrations of ferrimagnetic minerals, such as magnetite, and increases in the MS, M_r and M_s and SIRM. Therefore, the levels of M_r and M_s also may reflect the variation of the summer monsoon. The correlation coefficients of MS to M_r, M_s and SIRM are >0.85 (Table 3), which supports the close relationship among them.

Judging from the stratigraphy (L33, L15, L9, S5) and rock magnetic variations, we can divide the last 3 million years of paleoenvironmental history into four stages (I–IV) that correspond to the major stages in the evolution of the East Asian monsoon.

During Stage IV (3–2.6 Ma), the MS and M_r, M_s, SIRM and HIRM levels fluctuated synchronously with progressively larger amplitudes,

https://doi.org/10.1016/j.yqres.2013.10.002 Published online by Cambridge University Press

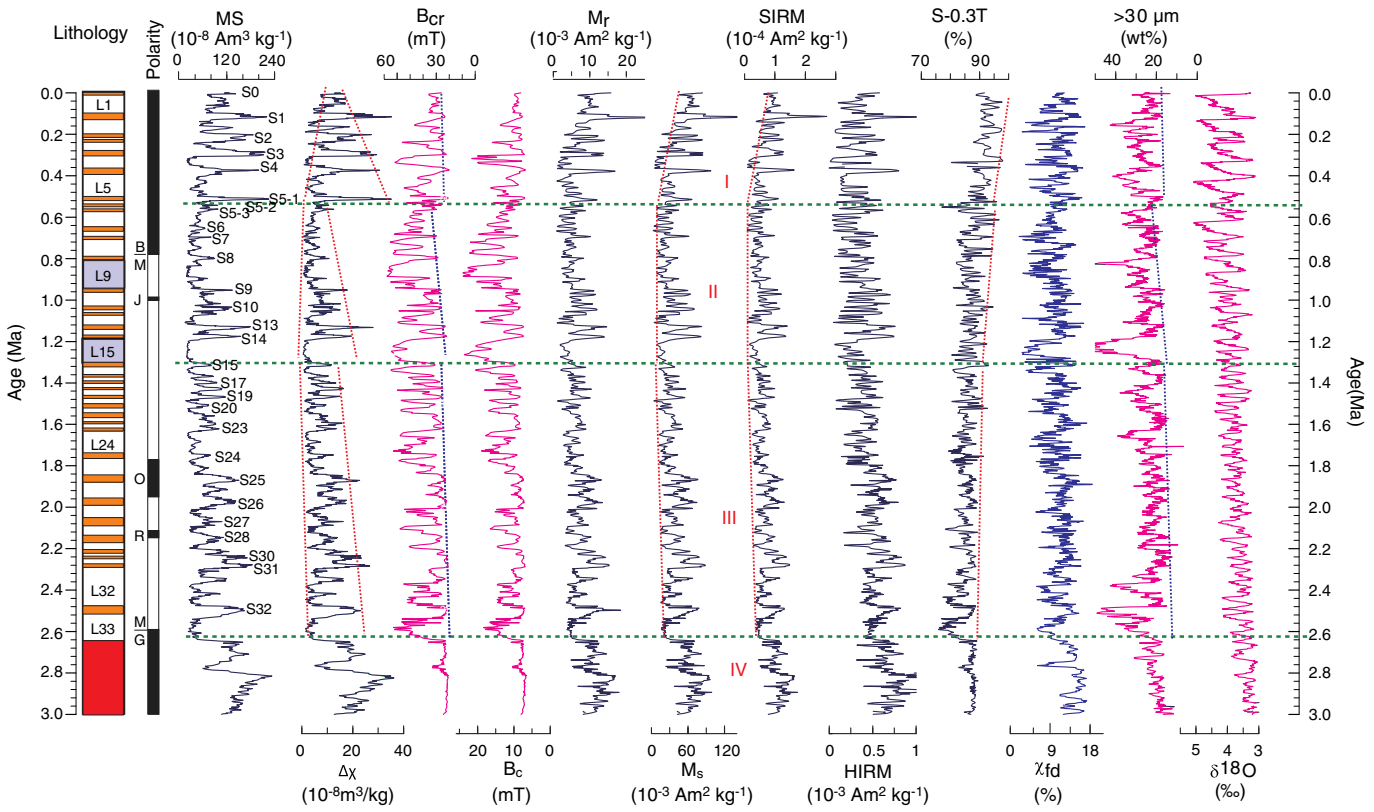

Figure 5. Time series of various rock magnetic parameters in the Chaona section.

whereas the Bcr, Bc and grain size (>30 μm) displayed a slightly increasing trend. The MS enhancement in the red-clay sequence revealed that the MS may be regarded as a proxy for the intensity of the East Asian summer monsoon (Nie et al., 2007) and even for the paleo-precipitation intensity on the CLP (Nie et al., 2008a). The MS values increased rapidly until 2.8 Ma, indicating a significantly intensified summer monsoon. Pollen assemblages of typical *Cupressaceae* forest vegetation in this section also indicate a relatively warm and humid climate during the late Pliocene (Wu et al., 2007). After 2.8 Ma, the MS level dropped abruptly, which suggests that the climate became drier (Wu et al., 2007) or the atmospheric circulation was rearranged (Ding et al., 2000). At the same time, the concentration of >30-μm particles displays an increasing trend (Fig. 5), which indicates the intensification of the winter monsoon. We infer that both the summer and winter monsoons strengthened during this interval against a background of an increasing volume of global ice (Lisiecki and Raymo, 2005) (Fig. 5).

It is hard to interpret the enhancement of the East Asia summer monsoon, given a simultaneous increase in the ice volume. Uplift of the Tibetan Plateau during this interval may have intensified the summer monsoonal precipitation by increasing the sea–land pressure gradient (An et al., 2001; Nie et al., 2008b). The abrupt change at approximately 2.6–2.8 Ma is consistent with the lithological transition from red-clay deposition to the development of the loess–paleosol sequence and coincided with the onset of major Northern Hemisphere glaciation, implying a rearrangement of the air-circulation (Ding et al., 2000; Sun et al., 2006a; Song et al., 2007).

During Stage III (2.6–1.3 Ma), cyclical changes were most prominent. There were four large cycles ~300–400-kyr long (Table 2) overprinted with several smaller cycles. The summer monsoon (reflected by the values of MS, Δχ, M_r, M_s, SIRM and HIRM) exhibited a long-term decreasing trend in the large-amplitude variability, which indicates a stepwise drying process. In contrast, the B_{cr} and B_c values exhibit a stepwise increase, indicating a gradual strengthening of the winter monsoon. However, the mean values and amplitudes of the $S_{-0.3\ T}$, χ_{fd} and amount of >30-μm particles were relatively stable over this interval.

During Stage II (1.3–0.6 Ma), two typical loess layers (L15, L9) developed. These layers display lower MS and higher amounts of coarse silt, which suggests the occurrence of important climatic or tectonic events. The upper silt layer (L9) (Liu et al., 1986) may be used to divide this interval into two parts. Below marker L9, the levels of magnetic parameters, such as MS, Ms, Mr, SIRM, HIRM, are relatively high, and the levels of Bcr and Bc and the coarse grain size are relatively low. Above marker L9, the levels of the various proxies fluctuate smoothly. The magnetic records indicate that the variation in the summer monsoon is asynchronous with that of the winter monsoon.

During Stage I (0.6 Ma–present), the amplitudes of MS, M_r, M_s and χ_{fd} increased significantly after 0.53 Ma (at the beginning of S5-1), which coincided approximately with the onset of large-amplitude glacial–interglacial cycles (Fig. 5). However, the initiation of significant increasing (decreasing) trends in the M_r, M_s, SIRM and HIRM occurred at 0.4 Ma. At that time, the summer monsoon was greatly enhanced. The winter monsoon, as reflected by an increasing trend in the B_{cr} and B_c values and grain size, increased both in mean intensity and amplitude.

Implication for the middle Pleistocene climate transition

The MPT was a complex global change leading to the late Pleistocene ice ages, with increased mean ice volume and a dominant 100-kyr cycle (Mudelsee and Stattegger, 1997). Recent studies suggest that the 400- and 100-kyr eccentricity cycles were clearly preserved in the loess–paleosol sequences (Nie, 2011), as were the periodicities in the obliquity (41-kyr) and precession (23 and 19-kyr) bands (Sun et al., 2006b; Han et al., 2012) revealed by the astronomical tuned time scale (Table 2). Our results, which are based on an independent time scale, confirm the existence of periods of approximately 400, 100, and 40-kyr, which indicates that the observed climate change may be related to variations in solar insolation. Problems remain, however, particularly with the

https://doi.org/10.1016/j.yqres.2013.10.002 Published online by Cambridge University Press

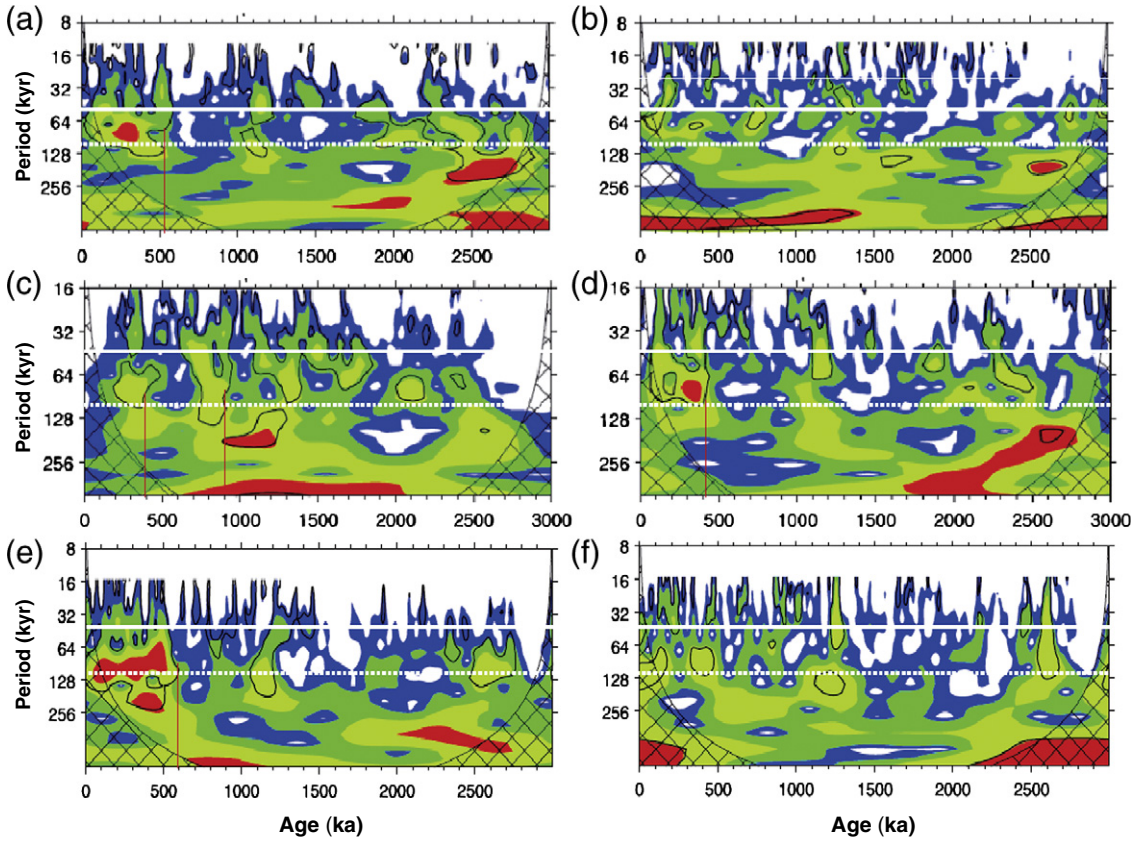

Figure 6. The wavelet power spectrum (Torrence and Compo, 1998) of (a) χ_{lf}, (b) χ_{fd}, (c) B_c, (d) M_s. (e) stacked χ and (f) stacked grain size. The contour levels are chosen so that 75%, 50%, 25%, and 5% of the wavelet power is above each level, respectively. The cross-hatched region is the cone of influence, where zero padding has reduced the variance. The black contour shows the 10% significance level, using a red-noise (autoregressive lag) background spectrum. The white solid and dashed lines represent the periods ~40 and ~100 -kyr, respectively. The stacked data (e, f) are from Sun et al. (2006b).

continuity of the 100-kyr signal during the MPT. The wavelet power spectrum indicates that the significant period of ~100-kyr appeared at ~1.2–1.3 Ma (in L15), disappeared between ~0.88 Ma and 0.53 Ma (between L9 and S5-1), and reappeared at ~0.53–0.46 Ma (in S5-1) (Figs. 6a, c, d). Spectral analysis (Fig. 7, Table 2) yields similar results and indicates that the ~100-kyr periods began to dominate after 1.2 Ma, disappeared at ~0.9 Ma, and then reappeared and dominated after 0.6 Ma. To explore the amplitude and variability of the 100-kyr period, we filtered these parameters with the 100-kyr bands using a Macintosh software program, AnalySeries (Paillard et al., 1996) (Fig. 8). The majority of the rock proxies, except Bc, exhibit no clear 100-kyr period before the MPT. The onset of a stable and clear 100-kyr period occurred at ~0.53 Ma (S5-1) (Figs. 8a–e) or 0.4 Ma (Fig. 8f).

If we take the emergence of the ~100-kyr period to be the beginning of the MPT and the stabilization of the 100-kyr period to be the end of the MPT, then the MPT interval occurred in the Chaona loess section from ~1.26 Ma to ~0.53 Ma (Figs. 8, 9), which corresponds to the zone from marker L15 to marker S5-1. It is notable that the ~100-kyr period in the marine oxygen isotope record emerged at ~0.68 Ma in LR04 (Fig. 8 h) or ODP677 (Fig. 9b) and at ~0.95 Ma in DSDP607 (Fig. 9d), but that a stable 100-kyr period in the global ice volume (Fig. 9c) emerged at approximately 0.88 Ma. The period of solar insolation at 65 °N is predominantly ~40-kyr long (Fig. 9e).

It is necessary to point that the grain-size age model has some assumption conditions. It assumes that coarse-grain-size maxima in the loess–palaeosol succession mark times when the competency and capacity of dust-bearing winds increased (Porter and An, 1995). In other words, there were two components in eolian deposition in Chinese loess. One is fine component with stable flux rate, while the other is coarse component with variable flux rate. In fact, the flux rate of fine component maybe also vary with time, the details of this quantitative relationship should be explored further. Therefore, the grain-size age time series may have some influences on periodical analyses. However, the grain-size age model is more reliable than linear interpolation method (Porter and An, 1995; Lu et al., 2004) and can provide a new insight about the climatic periodical changes.

A long-term cooling trend is often considered responsible for the changes in glacial dynamics during the MPT (Lisiecki and Raymo,

Table 2
Periods of various time intervals (kyr). Stacked MS and mean grain size data are from Sun et al. (2006b).

	0–2600 ka				1300–2600 ka			900–1400 ka		500–1000 ka			0–600 ka		
χ_{lf}	97	72	130	379	83	122	297	100	38	53	27	226*	87	41	
χ_{fd}	73	61	32		32	42	150	100	38	72			74	32	
>30 μm	219	99	45		99	56	173	133		57			40	192	
B_c	76	42	198		91	41	408	100		50			99	36	
M_s	407	224	133		74	34	297	80	22	53	29		80	42	27
Mean	208	104	45		189	103	54	114		57	266*		40	192	
Stacked χ	97	198	41	347	417	77	41	266–133	53	114	266	53	101	40	
Stacked mean	41	72	30	198	86	122	40	133	41	53	266		106	40	

https://doi.org/10.1016/j.yqres.2013.10.002 Published online by Cambridge University Press

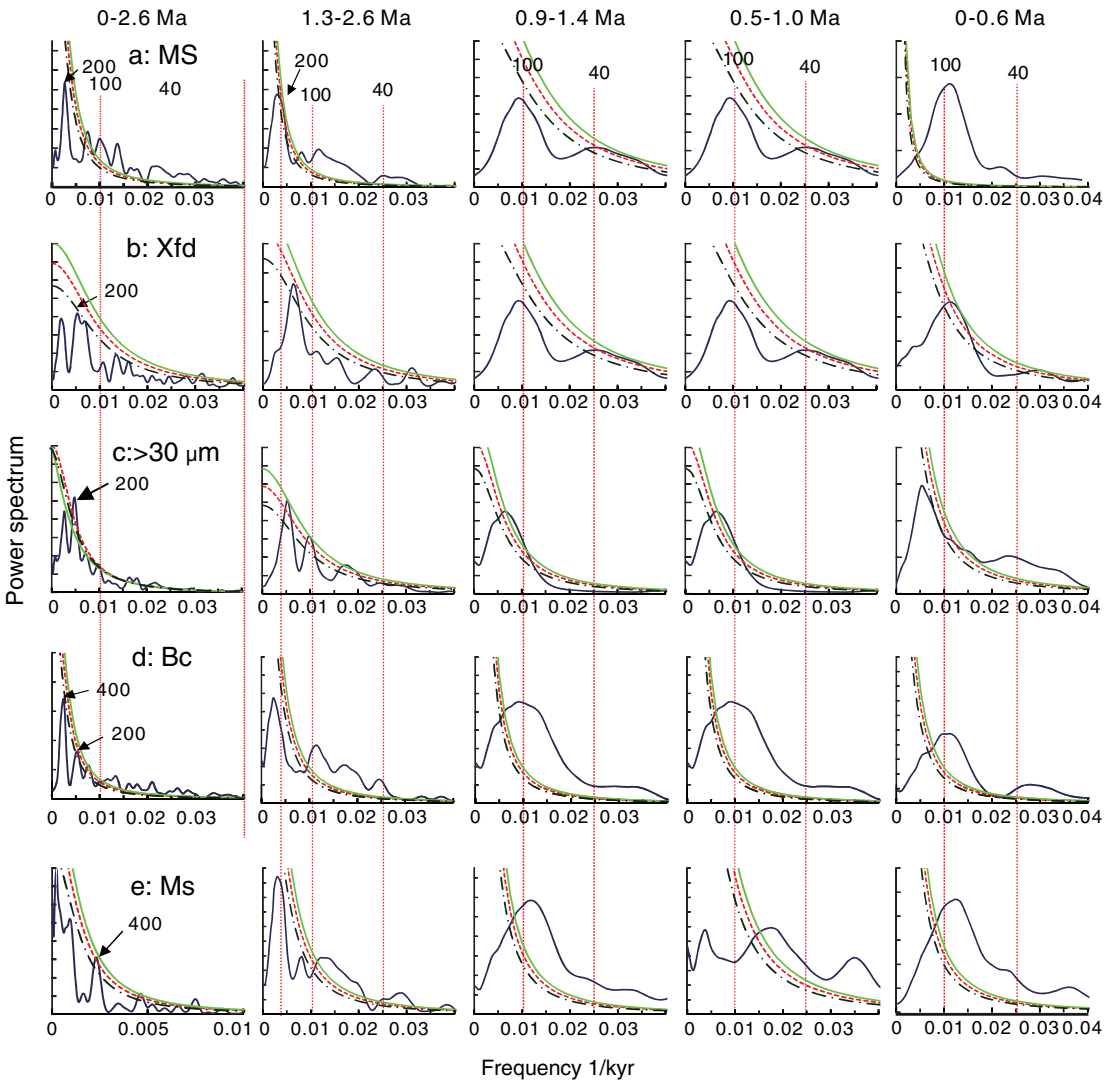

Figure 7. Power-spectrum analysis of the Chaona loess–paleosol sequences based on the program REDFIT 3.8 (Schulz and Mudelsee, 2002) (OFAC = 4, HIFAC = 1, n50 = 4, Iwin = Hanning, Nsim = 1000). Spectral analysis was performed at 4 time windows and for the entire time series. The blue, red and green lines indicate the 80%, 90% and 95% confidence levels, respectively.

2007), but the mechanisms responsible for the MPT are still controversial. There are several hypotheses, including decreasing atmospheric CO_2 (Clark et al., 2006), a sea-ice switch during glacial cycles (Tziperman and Gildor, 2003), weakening North Atlantic deep water circulation (Schmieder et al., 2000), a gradual increase in ice volume, uplift of the Tibetan Plateau (Fang et al., 1999) and a gradual increase in the threshold for ice-sheet ablation (Raymo et al., 1997).

The long-term variability and amplitudes of the 100-kyr filtered record of various rock magnetic proxies (Figs. 8a, c–e) are similar to the record of global ice volume (Fig. 8h) and differ from that of the solar insolation (Fig. 8i). This observation supports the hypothesis that the CLP is primarily influenced by the ice volume. However, the global ice volume cannot explain the changes observed in the MPT interval. The summer monsoon intensified suddenly at approximately ~1.2 Ma (Figs. 8a–d), whereas the winter monsoon decreased in intensity at approximately 1.26 Ma (Figs. 8f, g), and the global ice volume increased rapidly at ~1.25 Ma (Fig. 8h). It is very difficult to explain the summer monsoon strengthening and winter monsoon

Table 3
Correlation coefficients among rock magnetic parameters.

	χ_{lf}	χ_{hf}	$\Delta\chi$	B_{cr}	B_c	M_r	M_s	SIRM	HIRM	$S_{-0.3\,T}$	χ_{fd}	>30 μm
χ_{lf}	1.000											
χ_{hf}	0.998	1.000										
$\Delta\chi$	0.926	0.899	1.000									
B_{cr}	−0.812	−0.812	−0.743	1.000								
B_c	−0.763	−0.762	−0.698	0.965	1.000							
M_r	0.845	0.844	0.774	−0.734	−0.686	1.000						
M_s	0.864	0.865	0.783	−0.743	−0.704	0.982	1.000					
SIRM	0.854	0.854	0.784	−0.741	−0.691	0.972	0.964	1.000				
HIRM	0.548	0.542	0.531	−0.551	−0.535	0.770	0.698	0.783	1.000			
$S_{-0.3\,T}$	0.444	0.451	0.367	−0.381	−0.319	0.264	0.348	0.275	−0.323	1.000		
χ_{fd}	0.431	0.382	0.668	−0.454	−0.462	0.364	0.351	0.371	0.332	0.106	1.000	
>30 μm	−0.147	−0.145	−0.141	0.232	0.216	−0.212	−0.188	−0.194	−0.203	0.003	−0.159	1.000

https://doi.org/10.1016/j.yqres.2013.10.002 Published online by Cambridge University Press

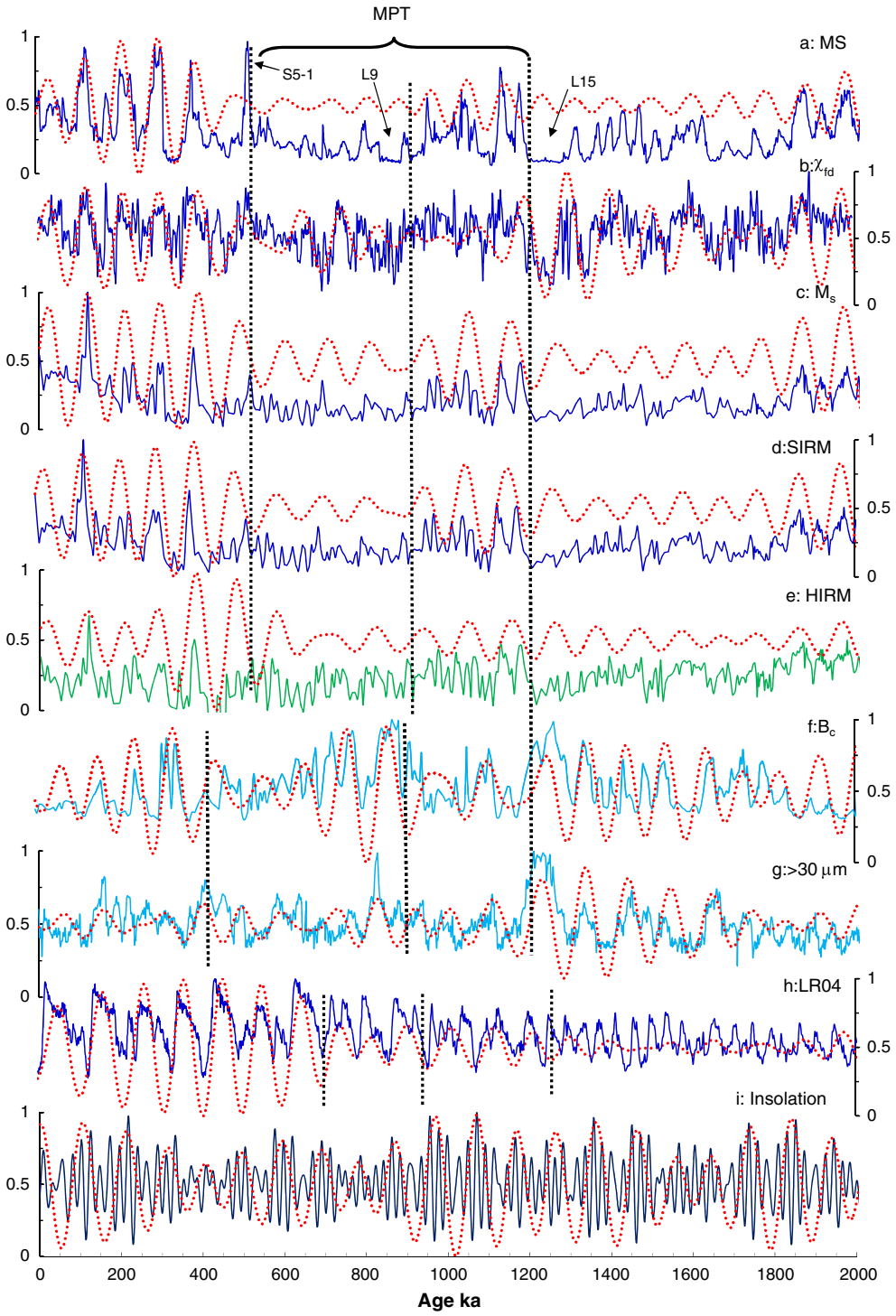

Figure 8. The timing and structure during the middle Pleistocene climate transition interval recorded in the Chaona loess–paleosol sequence and their 100-kyr band variability and correlations. East Asia summer monsoon proxies a: χ_{lf}, b: χ_{fd}, c: M_s, d: SIRM; Winter monsoon proxies e: HIRM, f: Bc, g:. > 30 μm; h: global stacked oxygen isotope curve (LR04) (Lisiecki and Raymo, 2005) and i: solar insolation at 65°N (Berger and Loutre, 1991). All data were normalized at (0,1). Red line denotes 10-kyr band filtering using AnalySeries 2.0 (Paillard et al., 1996). Dashed line denotes the onset or disappearance of the 10^6-kyr period.

weakening by the increase in the ice volume. An increasing ice volume will tend to cause global cooling, which would tend to intensify the winter monsoon and not the summer monsoon. It seems likely that the global ice volume is not the primary factor controlling the MPT in the CLP. Solar insolation in the Northern Hemisphere also exhibits a relatively weak period (Fig. 8i) that is not enough to cause the observed climate change.

The sudden change may be related to an important abrupt event. We consider the most likely factor that triggered the MPT in the CLP to be the uplift of the Tibetan Plateau. Geological evidence indicates that the L15 coarser silt event was the result of uplift of the Tibetan Plateau (Sun and Liu, 2000; Sun and An, 2005). From the late Pliocene to the early Pleistocene, a series of lakes was distributed across north-central China, primarily on the CLP. However, at ~1.1 Ma these lakes evaporated, and

https://doi.org/10.1016/j.yqres.2013.10.002 Published online by Cambridge University Press

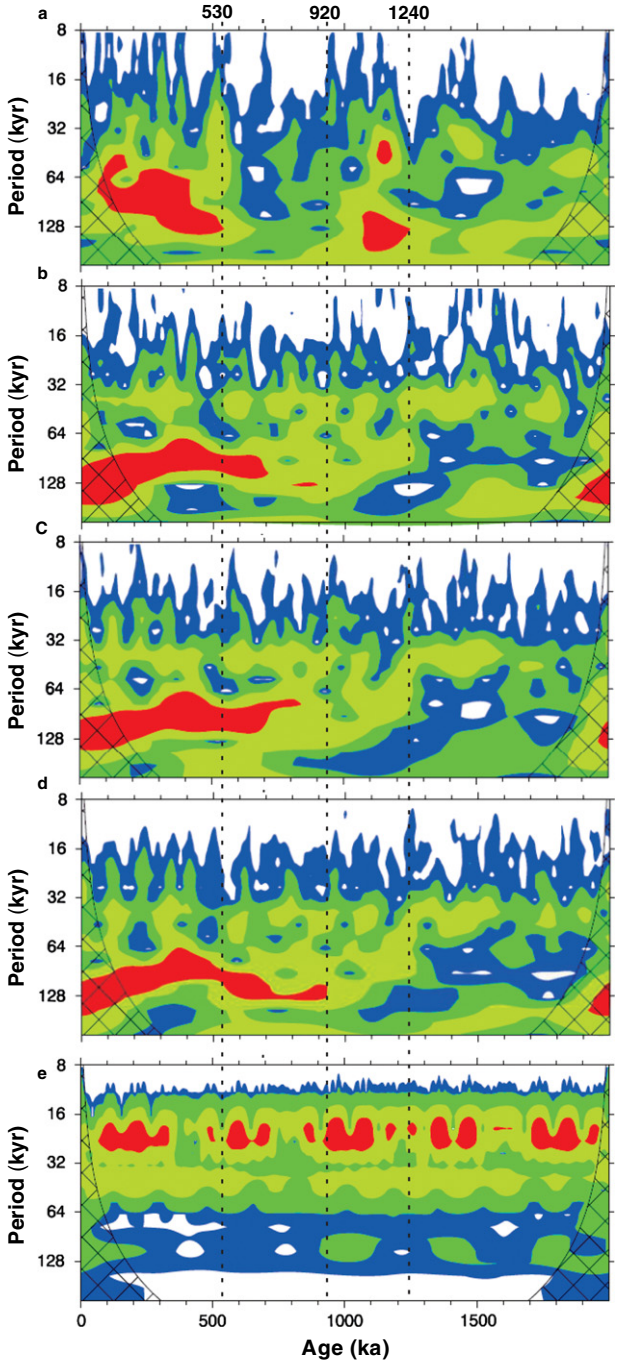

Figure 9. The wavelet power spectrum (Torrence and Compo, 1998) of (a) χ_{lf}, (b) ODP677 (Shackleton et al., 1990), (c) LR04 stack (Lisiecki and Raymo, 2005), (d) DSDP607 (Raymo et al., 1997), (e) Solar insolation at 65°N (Berger and Loutre, 1991). The contour levels are chosen so that 75%, 50%, 25%, and 5% of the wavelet power is above each level, respectively. The cross-hatched region is the cone of influence, where zero padding has reduced the variance. White solid lines show the age of onset of the ~100-kyr period.

lacustrine deposition was replaced by subsequent loess deposition (Sun and Liu, 2000). The disappearance of these lakes was most likely associated with mountain uplift and incision by the Yellow River at 1.1 Ma, as indicated by the widespread Yellow River terrace of this period (Li, 1991; Li et al., 1997). The rapid middle Pleistocene uplift of the Tibetan Plateau is called the Kunlun-Yellow River (KYR) Movement (Cui et al., 1998), which consisted of three episodes starting at 1.2 Ma, 0.9–0.8 Ma and 0.6 Ma. Many indications of this KYR tectonic movement have been found in the northern and northeastern Tibetan Plateau and its adjacent areas (Fang et al., 2005; Pan et al., 2007; Liu et al., 2010).

The rapid middle Pleistocene uplift of the Tibetan Plateau may have caused the altitude to reach a threshold value for influencing atmospheric circulation conditions and the rates of weathering and erosion. The role that the Tibetan Plateau plays as a heat sink during the winter and a heat source during the summer (An et al., 2001) has a great effect on the climate in northwest China. The thermal forcing of the Tibetan Plateau intensifies the East Asian summer monsoon to the east and in the dry Gobi desert to the west, which brings more precipitation to the CLP. The uplifted plateau and altered circulation may have strengthened the intensity of the Siberian High and the winter monsoon (Han et al., 2012), which brought more eolian sediments to the CLP. It also may have bifurcated the low-level westerlies around the plateau and strengthened northward movement of the northern branch of the westerlies (Fang et al., 1999).

Conclusions

1. Statistical analyses of data from the CLP loess–paleosol sequence indicate that the loess levels are characterized by relatively higher coercivity (B_c), remanent coercivity (B_{cr}), lower MS (χ_{lf}) and coarser grain-size and that the paleosol levels are characterized by relatively high χ_{lf}, saturation magnetization (M_s), remanent saturation magnetization (M_r) and finer grain size.
2. In terms of the stratigraphy and magnetic records, the paleo-environmental evolution during the last 3 Ma may be divided into four key intervals, designated I–IV: 0–0.6, 0.6–1.3, 1.3–2.6, and 2.6–3.0 Ma.
3. Our analyses, which was based on a newly developed independent time scale (not orbitally tuned), indicate that, in addition to the usual orbital periods of 100, 41, and 21-kyr, there are non-orbital periods. The MPT in the Chaona loess_paleosol sequence began ~1.26 Ma and ended by ~0.53 Ma, which is a conclusion that differs from those of previous investigations based on orbitally tuned time scales. The mechanism driving the MPT was more complex than just the orbital forcing. We conclude that the rapid uplift of the Tibetan Plateau may have played an important role in the shift of periodicities during the MPT.

Acknowledgments

This study was co-supported by the Natural Science Foundation of China (Nos. 41172166, 41290253) and the National Basic Research Program of China (2013CB955904, 2010CB833403). Y. G. Song gratefully thanks Prof. Masuyuki Torii and Dr. Su Li for laboratory guidance. We thank Profs. Lu Huayu, Mike Dekker, Guillaume Dupont-Nivet and Junsheng Nie for valuable comments on an early draft of the manuscript. Special thanks to guest editor Prof. Fafu Chen and the two anonymous reviewers for their critical comments, which significantly improved this paper.

References

An, Z.S., 2000. The history and variability of the East Asian paleomonsoon climate. Quaternary Science Reviews 19, 171–187.
An, Z.S., Liu, T.S., Lu, Y.C., Porter, S.C., Kukla, G., Wu, X.H., Hua, Y.M., 1990. The long-term paleomonsoon variation recorded by the loess-paleosol sequence in Central China. Quaternary International 7–8, 91–95.
An, Z.S., Kukla, G.J., Porter, S.C., Xiao, J.L., 1991. Magnetic susceptibility evidence of monsoon variation on the Loess Plateau of central China during the last 130,000 years. Quaternary Research 36, 29–36.
An, Z.S., Kutzbach, J.E., Prell, W.L., Porter, S.C., 2001. Evolution of Asian monsoons and phased uplift of the Himalaya-Tibetan plateau since Late Miocene times. Nature 411, 62–66.
Berger, A., Loutre, M.F., 1991. Insolation values for climate of the last 10 million years. Quaternary Science Reviews 10, 297–317.
Berger, A., Li, X.S., Loutre, M.F., 1999. Modelling northern hemisphere ice volume over the last 3 Ma. Quaternary Science Reviews 18, 1–11.
Bloemendal, J., Liu, X., 2005. Rock magnetism and geochemistry of two plio-pleistocene Chinese loess-palaeosol sequences–implications for quantitative palaeoprecipitation reconstruction. Palaeogeography, Palaeoclimatology, Palaeoecology 226, 149–166.

Clark, P.U., Archer, D., Pollard, D., Blum, J.D., Rial, J.A., Brovkin, V., Mix, A.C., Pisias, N.G., Roy, M., 2006. The middle Pleistocene transition: characteristics, mechanisms, and implications for long-term changes in atmospheric pCO2. Quaternary Science Reviews 25, 3150–3184.
Cui, Z., Wu, Y., Liu, G., Ge, D., Pang, Q., Xu, Q., 1998. On Kunlun-Yellow River tectonic movement. Science in China Series D: Earth Sciences 41, 592–600.
Day, R., Fuller, M., Schmidt, V.A., 1977. Hysteresis properties of titanomagnetites: grain-size and compositional dependence. Physics of the Earth and Planetary Interiors 13, 260–267.
Dekkers, M.J., 1997. Environmental magnetism, an introduction. Geologie en Mijnbouw 76, 163–182.
Deng, C., Vidic, N.J., Verosub, K.L., Singer, M.J., Liu, Q., Shaw, J., Zhu, R., 2005a. Mineral magnetic variation of the Jiaodao Chinese loess/paleosol sequence and its bearing on long-term climatic variability. Journal of Geophysical Research 110, 1–17.
Deng, C., Vidic, N.J., Verosub, K.L., Singer, M.J., Liu, Q., Shaw, J., Zhu, R., 2005b. Mineral magnetic variation of the Jiaodao Chinese loess/paleosol sequence and its bearing on long-term climatic variability. Journal of Geophysical Research - Solid Earth 110, B03103. http://dx.doi.org/10.1029/2004JB003451.
Ding, Z., Yu, Z., Rutter, N.W., Liu, T., 1994. Towards an orbital time scale for Chinese loess deposits. Quaternary Science Reviews 13, 39–70.
Ding, Z.L., Rutter, N.W., Sun, J.M., Yang, S.L., Liu, T.S., 2000. Re-arrangement of atmospheric circulation at about 2.6 Ma over northern China: evidence from grain size records of loess-palaeosol and red clay sequences. Quaternary Science Reviews 19, 547–558.
Dunlop, D.J., Özdemir, Ö., 1997. Rock Magnetism: Fundamentals and Frontiers. Cambridge Univ. Press, New York.
Evans, M.E., Heller, F., 2001. Magnetism of loess/palaeosol sequences: recent developments. Earth-Science Reviews 54, 129–144.
Evans, M.E., Rokosh, C.D., Rutter, N.W., 2002. Magnetoclimatology and paleoprecipitation: evidence from a north-south transect through the Chinese Loess Plateau. Geophysical Research Letters 29, 127-121–127-124.
Fang, X.M., Li, J.J., Van der Voo, R., 1999. Rock magnetic and grain size evidence for intensified Asian atmospheric circulation since 800,000 years B.P. related to Tibetan uplift. Earth and Planetary Science Letters 165, 129–144.
Fang, X., Yan, M., Van der Voo, R., Rea, D.K., Song, C., Parés, J.M., Gao, J., Nie, J., Dai, S., 2005. Late Cenozoic deformation and uplift of the NE Tibetan Plateau: evidence from high-resolution magnetostratigraphy of the Guide Basin, Qinghai Province, China. Geological Society of America Bulletin 117, 1208–1225.
Fukuma, K., Torii, M., 1998. Variable shape of magnetic hysteresis loops in the Chinese loess-paleosol sequence. Earth Planetary Space 50, 9–14.
Han, W., Fang, X., Berger, A., Yin, Q., 2011. An astronomically tuned 8.1 Ma eolian record from the Chinese Loess Plateau and its implication on the evolution of Asian monsoon. Journal of Geophysical Research 116, D24114. http://dx.doi.org/10.1029/22011jd016237.
Han, W., Fang, X., Berger, A., 2012. Tibet forcing of mid-Pleistocene synchronous enhancement of East Asian winter and summer monsoons revealed by Chinese loess record. Quaternary Research 78, 174–184.
Hao, Q., Oldfield, F., Bloemendal, J., Torrent, J., Guo, Z., 2009. The record of changing hematite and goethite accumulation over the past 22 Myr on the Chinese Loess Plateau from magnetic measurements and diffuse reflectance spectroscopy. Journal of Geophysical Research - Solid Earth 114, B12101. http://dx.doi.org/10.1029/2009JB006604.
Hao, Q.Z., Wang, L., Oldfield, F., Peng, S.Z., Qin, L., Song, Y., Xu, B., Qiao, Y.S., Bloemendal, J., Guo, Z.T., 2012. Delayed build-up of Arctic ice sheets during 400,000-year minima in insolation variability. Nature 490, 393–396.
Heller, F., Liu, T.S., 1986. Paleoclimatic and sedimentary history from magnetic susceptibility of loess in China. Geophysical Research Letters 13, 1169–1172.
Heller, F., Shen, C.D., Beer, J., Liu, X.M., Liu, T.S., Bronger, A., Suter, M., Bonani, G., 1993. Quantitative estimates of pedogenic ferromagnetic mineral formation in Chinese loess and palaeoclimatic implications. Earth and Planetary Science Letters 114, 385–390.
Heslop, D., Langereis, C.G., Dekkers, M.J., 2000. A new astronomical timescale for the loess deposits of Northern China. Earth and Planetary Science Letters 184, 125–139.
Heslop, D., Dekkers, M.J., Langereis, C.G., 2002. Timing and structure of the mid-Pleistocene transition: records from the loess deposits of northern China. Palaeogeography, Palaeoclimatology, Palaeoecology 185, 133–143.
Hunt, C.P., Banerjee, S.K., Han, J.M., Solheid, P.A., Oches, E.A., Sun, W., Liu, T., 1995. Rock-magnetic proxies of climate change in the loess-paleosol sequences of the western Loess Plateau of China. Geophysical Journal International 123, 232–244.
King, J.W., Channell, J.E.T., 1990. Sedimentary magnetism, environmental magnetism, and magnetostratigraphy. Reviews of Geophysics 29, 358–370.
Kukla, G., 1987. Loess stratigraphy in central China. Quaternary Science Reviews 6, 191–207 (209–219).
Li, J., 1991. The environmental effects of the uplift of the Qinghai-Xizang Plateau. Quaternary Science Reviews 10, 479–483.
Li, J.J., Fang, X.M., Van der Voo, R., Zhu, J.J., Niocaill, C.M., Ono, Y., Pan, B.T., Zhong, W., Wang, J.L., Sasaki, T., Zhang, Y.T., Cao, J.X., Kang, S.C., Wang, J.M., 1997. Magnetostratigraphic dating of river terraces: rapid and intermittent incision by the Yellow River of the northeastern margin of the Tibetan Plateau during the Quaternary. Journal of Geophysical Research - Solid Earth 102, 10121–10132.
Lisiecki, L.E., Raymo, M.E., 2005. A Pliocene-Pleistocene stack of 57 globally distributed benthic δ18O records. Paleoceanography 20, PA1003. http://dx.doi.org/10.1029/2004PA001071.
Lisiecki, L., Raymo, M.E., 2007. Plio-Pleistocene climate evolution: trends and transitions in glacial cycle dynamics. Quaternary Science Reviews 26, 56–69.
Liu, T., Zhang, S., Han, J., 1986. Stratigraphy and paleoenvironmental changes in the loess of central China. Quaternary Science Reviews 5, 489–495.
Liu, X.M., Shaw, J., Heller, F., Yuan, B.Y., 1992. Magnetic mineralogy of Chinese loess and its significance. Geophysical Journal International 108, 301–308.
Liu, Q., Deng, C., Torrent, J., Zhu, R., 2007. Review of recent developments in mineral magnetism of the Chinese loess. Quaternary Science Reviews 26, 368–385.
Liu, D., Fang, X., Song, C., Dai, S., Zhang, T., Zhang, W., Miao, Y., Liu, Y., Wang, J., 2010. Stratigraphic and paleomagnetic evidence of mid-Pleistocene rapid deformation and uplift of the NE Tibetan Plateau. Tectonophysics 486, 108–119.
Lourens, L., Hilgen, F., Shackleton, N.J., Laskar, J., Wilson, D., 2004. The Neogene Period. In: Gradstein, F., Ogg, J., Smith, A.G. (Eds.), Geologic Time Scale. Cambridge University Press, Cambridge, pp. 409–440.
Lu, H., Liu, X., Zhang, F., An, Z., Dodson, J., 1999. Astronomical calibration of loess-paleosol deposits at Luochuan, central Chinese Loess Plateau. Palaeogeography, Palaeoclimatology, Palaeoecology 154, 237–246.
Lü, L., Fang, X., Joseph, A.M., Li, J., An, Z., 2001. The evolution of coupling of Asian winter monsoon and high latitude climate of Northern Hemisphere: grain evidence from 8.1 Ma loess-red clay sequence on the Chinese central Loess Plateau. Science in China Series D: Earth Sciences 44, 185–191.
Lu, H., Zhang, F., Liu, X., 2003. Patterns and frequencies of the East Asian winter monsoon variations during the past million years revealed by wavelet and spectral analyses. Global and Planetary Change 35, 67–74.
Lu, H., Zhang, F., Liu, X., Duce, R.A., 2004. Periodicities of palaeoclimatic variations recorded by loess-paleosol sequences in China. Quaternary Science Reviews 23, 1891–1900.
Lu, Y.C., Wang, X.L., Wintle, A.G., 2007. A new OSL chronology for dust accumulation in the last 130,000 yr for the Chinese Loess Plateau. Quaternary Research 67, 152–160.
Maher, B.A., Thompson, R., 1992. Paleoclimatic significance of the mineral magnetic record of the Chinese loess and paleosols. Quaternary Research 37, 155–170.
Maher, B.A., Thompson, R., 1995. Paleorainfall reconstructions from pedogenic magnetic susceptibility variations in the Chinese loess and paleosols. Quaternary Research 44, 383–391.
Maher, B.A., Tompson, R., 1992. Plaeomagnetic significance of the mineral magnetic record of the Chinese loess and paleosols. Quaternary Research 37, 155–170.
Maher, B.A., Thompson, R., Zhou, L.P., 1994. Spatial and temporal reconstructions of changes in the Asian palaeomonsoon: a new mineral magnetic approach. Earth and Planetary Science Letters 125, 461–471.
Maher, B.A., Mutch, T.J., Cunningham, D., 2009. Magnetic and geochemical characteristics of Gobi Desert surface sediments: implications for provenance of the Chinese Loess Plateau. Geology 37, 279–282.
Mudelsee, M., Schulz, M., 1997. The Mid-Pleistocene climate transition: onset of 100 ka cycle lags ice volume build-up by 280 ka. Earth and Planetary Science Letters 151, 117–123.
Mudelsee, M., Stattegger, K., 1997. Exploring the structure of the mid-Pleistocene revolution with advanced methods of time-series analysis. Geologische Rundschau 86, 499–511.
Nie, J.S., 2011. Coupled 100-kyr cycles between 3 and 1 Ma in terrestrial and marine paleoclimatic records. Geochemistry, Geophysics, Geosystems 12, Q10Z32. http://dx.doi.org/10.1029/2011GC003772.
Nie, J.S., King, J.W., Fang, X.M., 2007. Enhancement mechanisms of magnetic susceptibility in the Chinese red-clay sequence. Geophysical Research Letters 34, L19705. http://dx.doi.org/10.1029/2007GL031430.
Nie, J.S., King, J.W., Fang, X.M., 2008a. Correlation between the magnetic susceptibility record of the Chinese aeolian sequences and the marine benthic oxygen isotope record. Geochemistry, Geophysics, Geosystems 9, Q12026. http://dx.doi.org/10.1029/2008GC002243.
Nie, J.S., King, J.W., Fang, X.M., 2008b. Link between benthic oxygen isotopes and magnetic susceptibility in the red-clay sequence on the Chinese Loess Plateau. Geophysical Research Letters 35, L03703. http://dx.doi.org/10.1029/2007GL032817.
Nie, J.S., Song, Y.G., King, J.W., Egli, R., 2010. Consistent grain size distribution of pedogenic maghemite of surface soils and Miocene loessic soils on the Chinese Loess Plateau. Journal of Quaternary Science 25, 261–266.
Paillard, D., Labeyrie, L., Yiou, P., 1996. Analyseries 1.0: a Macintosh software for the analysis of geographical time-series. EOS 77, 379.
Pan, B.T., Gao, H.S., Wu, G.J., Li, J.J., Li, B.Y., Ye, Y.G., 2007. Dating of erosion surface and terraces in the eastern Qilian Shan, northwest China. Earth Surface Processes and Landforms 32, 143–154.
Porter, S.C., An, Z.S., 1995. Correlation between climate events in the North Atlantic and China during the last glaciation. Nature 375, 305–308.
Raymo, M.E., Oppo, D.W., Curry, W., 1997. The mid-Pleistocene climate transition: a deep sea carbon isotopic perspective. Paleoceanography 12, 546–559.
Ruddiman, W., Raymo, M., Martinson, D., Clement, B., Backman, J., 1989. Pleistocene evolution: Northern Hemisphere ice sheets and North Atlantic Ocean. Paleoceanography 4, 353–412.
Schmieder, F., Dobeneck, T.V., Bleil, U., 2000. The Mid-Pleistocene climate transition as documented in the deep South Atlantic Ocean: initiation, interim state and terminal event. Earth and Planetary Science Letters 179, 539–549.
Schulz, M., Mudelsee, M., 2002. REDFIT: estimating red-noise spectra directly from unevenly spaced paleoclimatic time series. Computers & Geosciences 28, 421–426.
Shackleton, N.J., Berger, A.J., Peltier, W.R., 1990. An alternative astronomical calibration of the lower Pleistocene timescale based on ODP Site 677. Transactions of the Royal Society of Edinburgh, Earth Science 81, 251–261.
Song, Y.G., Fang, X.M., Li, J.J., An, Z.S., Miao, X.D., 2001. The Late Cenozoic uplift of the Liupan Shan, China. Science in China Series D: Earth Sciences 44, 176–184.
Song, Y.G., Fang, X.M., Torii, M., Ishikawa, N., Li, J.J., An, Z.S., 2007. Late Neogene rock magnetic record of climatic variation from Chinese eolian sediments related to uplift of the Tibetan Plateau. Journal of Asian Earth Sciences 30, 324–332.

https://doi.org/10.1016/j.yqres.2013.10.002 Published online by Cambridge University Press

Sun, Y.B., An, Z.S., 2005. Late Pliocene-Pleistocene changes in mass accumulation rates of eolian deposits on the central Chinese Loess Plateau. Journal of Geophysical Research 110, D23101. http://dx.doi.org/10.1029/2005JD006064.
Sun, J.M., Liu, T.S., 2000. Stratigraphic evidence for the uplift of the Tibetan Plateau between 1.1 and 0.9 myr Ago. Quaternary Research 54, 309–320.
Sun, Y.B., Chen, J., Clemens, S.C., Liu, Q.S., Ji, J.F., Tada, R., 2006a. East Asian monsoon variability over the last seven glacial cycles recorded by a loess sequence from the northwestern Chinese Loess Plateau. Geochemistry, Geophysics, Geosystems 7, 1–16.
Sun, Y.B., Clemens, S.C., An, Z.S., Yu, Z.W., 2006b. Astronomical timescale and palaeoclimatic implication of stacked 3.6-Myr monsoon records from the Chinese Loess Plateau. Quaternary Science Reviews 25, 33–48.
Thompson, R., Oldfield, F., 1986. Environmental Magnetism. Allen & Unwin, London.
Torrence, C., Compo, G.P., 1998. A practical guide to wavelet analysis. Bulletin of the American Meteorological Society 79, 61–78.
Tziperman, E., Gildor, H., 2003. On the mid-Pleistocene transition to 100-kyr glacial cycles and the asymmetry between glaciation and deglaciation times. Paleoceanography 18, 1001. http://dx.doi.org/10.1029/2001PA000627 (002003).
Wu, F.L., Fang, X.M., Ma, Y.Z., Herrmann, M., Mosbrugger, V., An, Z.S., Miao, Y.F., 2007. Plio-Quaternary stepwise drying of Asia: evidence from a 3-Ma pollen record from the Chinese Loess Plateau. Earth and Planetary Science Letters 257, 160–169.
Zhou, L.P., Oldfield, F., Wintle, A.G., Robinson, S.G., Wang, J.T., 1990. Partly pedogenic origin of magnetic variations in Chinese loess. Nature 346, 737–739.

https://doi.org/10.1016/j.yqres.2013.10.002 Published online by Cambridge University Press